

1 *Conference Proceedings Paper*

2 **Assessment of flooding risk in Lima, Peru, through** 3 **change detection based on ERS-1/2 and Sentinel-1** 4 **time series**

5 Nancy Alvan Romero ^{1,2*}, Francesca Cigna ¹ and Deodato Tapete ^{1,*}

6 Published: date

7 Academic Editor: name

8 ¹ Italian Space Agency (ASI), Via del Politecnico s.n.c., 00133 Rome, Italy; francesca.cigna@asi.it

9 ² Mathematics Department, University of Rome "Tor Vergata", Via della Ricerca Scientifica 1, 00133 Rome,
10 Italy

11 * Correspondence: nalvanr@gmail.com (N.A.R.), deodato.tapete@asi.it (D.T.)

12 **Abstract:** Catastrophic floods that happened in Lima in 1997–1998 and 2017–2018 caused hundreds
13 of fatalities and significant economic loss. To test the hypothesis that information mined from
14 satellite synthetic aperture radar (SAR) images can provide valuable inputs into the common
15 workflow of flooding hazard assessment, the complete archives collected over the Rímac River
16 basin by the European Space Agency's ERS-1/2 missions and the European Commission's
17 Copernicus Sentinel-1 constellation were screened. SAR backscatter color composites and ratio
18 maps were created to identify change patterns occurred prior, during and after the catastrophic
19 flooding events mentioned above. A total of 409 areas (58.50 km²) revealing change were mapped,
20 including 197 changes (32.10 km²) due to flooding-related backscatter variations and 212 (26.40
21 km²) due to other processes (e.g., new urban developments, construction of river embankments,
22 other engineering works, vegetation changes). The areas inundated during the flooding events in
23 1997–1998 and 2017–2018 mostly concentrate along the riverbanks and plain, where low-lying
24 topography and gentle slopes ($\leq 5^\circ$), together with the presence of alluvial deposits, also indicate
25 greater susceptibility to flooding. Through geospatial integration with ancillary data (topography,
26 geology, permanent and seasonal water bodies, urban footprint, new urban development, roads
27 and infrastructure, and population at the district level), a risk classification map of Lima was
28 produced. The map highlights the sectors of potential concern along the Rímac River, should
29 flooding events of equal severity as those captured by SAR images occur in the future. Key findings
30 are presented in this short paper, while the full study is published in the journal *Applied Sciences*.

31 **Keywords:** flooding; synthetic aperture radar; change detection; radar backscatter; urban remote
32 sensing; GIS-based analysis; risk classification

34 1. Introduction

35 In recent years, Lima, the Peruvian capital, has experienced severe and catastrophic floods [1].
36 These events became more frequent, especially in the coastal area of the Peruvian mainland, as a
37 consequence of El Niño. A chronological long-term ground-based data analysis has allowed the
38 identification of major flooding events occurred in the last century along the Peruvian coast,
39 specifically in the areas near Lima. In particular, two main flooding events that occurred in
40 1997–1998 and 2017–2018 were selected as the focus of this study because, according to the
41 Emergency Events Database [2], they caused significant damage to urban infrastructure.

42 The aim of this research was to assess whether a flood risk map of the city could be generated
43 based on the evidence of flooded areas during these events, as recorded in satellite Synthetic

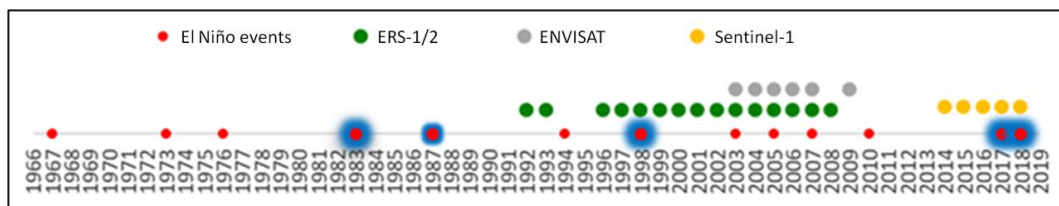
44 Aperture Radar (SAR) images. The basic processing workflow in order to achieve this goal consisted
 45 in pre and post-processing of SAR data, generation of RGB composites that showed “where” the
 46 change patterns occurred, and the ratio maps providing the information on the magnitude of such
 47 changes. These products jointly with three key spatial hazard datasets (terrain slope, alluvial
 48 deposits and land cover) and ancillary data related to topography, geology, urban footprint, roads
 49 and population, allowed us to undertake an integrated evaluation of the hazards and a risk analysis.

50 Key findings from this integrated analysis are presented in this paper. For the detailed analysis
 51 and discussion of the results, the reader can refer to the full article published in the journal *Applied*
 52 *Sciences* [3].

53 **2. Experiments**

54 Figure 1 shows the timeline of the El Niño events that were taken into account vs. the whole
 55 SAR archive images acquired by European Space Agency (ESA)’s European Remote-Sensing
 56 (ERS-1/2) [4] and Copernicus Sentinel-1 Interferometric Wide-Swath (IW) mode data [5] that were
 57 processed and analyzed. Given that no images collected by ESA’s ENVironmental SATellite
 58 (ENVISAT) satellite were available to cover any of the other El Niño-related events, these data were
 59 not used in the end.

60 Pre-, cross- and post-event SAR pairs were considered to investigate the 1997–1998 and
 61 2017–2018 flooding events affecting Lima (Table 1).



62
 63 **Figure 1.** Flood events and El Niño phenomenon vs. availability of C-band synthetic aperture radar
 64 (SAR) satellite data from ESA’s European Remote-Sensing (ERS-1/2), ENVironmental SATellite
 65 (ENVISAT), and Copernicus Sentinel-1 missions. The most intense events are indicated in blue. Full
 66 paper source: [3].

67 **Table 1.** SAR image working pairs made of ERS-1/2 and Sentinel-1 scenes over Lima, Peru.

SAR Image Working Pairs	Pre-Event	Cross-Event	Post-Event	Total
1997–1998	1	4	4	9
2017–2018	10	10	10	30

68 The SAR processing workflow ran in the Sentinel Application Platform (SNAP) v.6.0 software,
 69 using the Sentinel-1 toolbox (S1TBX), and included: (i) radiometric calibration and precise
 70 co-registration of the SAR scenes; (ii) terrain correction and geocoding to map coordinates; and (iii)
 71 generation of SAR amplitude color composites and ratio maps.

72 Hazard and risk analysis was conducted by combining SAR amplitude change patterns and
 73 geospatial data related to topography, geology, alluvial deposits, urban footprint, new urban
 74 development, roads and infrastructure, population at district level.

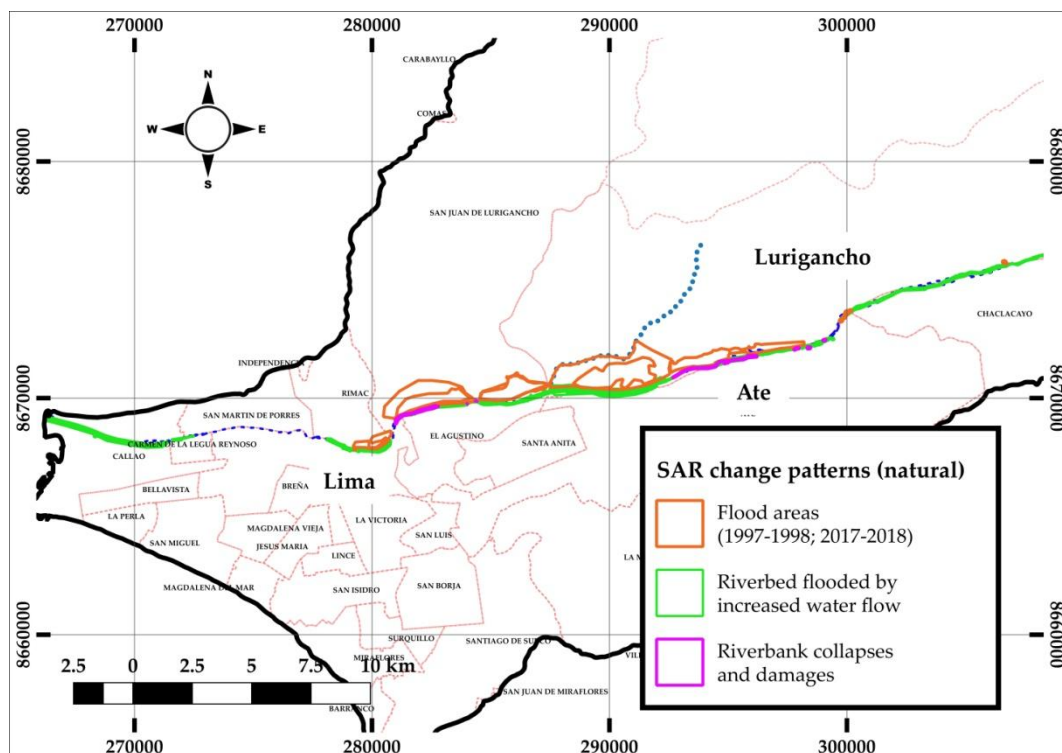
76 **3. Results**

77 A total of 197 changes attributed to the “Flooding” group were highlighted, for a total of 32.10
 78 km². These changes are distributed throughout the whole extent of the riverbed of the Rímac River
 79 and, as expected, also include the areas that have been affected by the flooding events occurred in
 80 the years 1997–1998 and 2017–2018 (Figure 2).

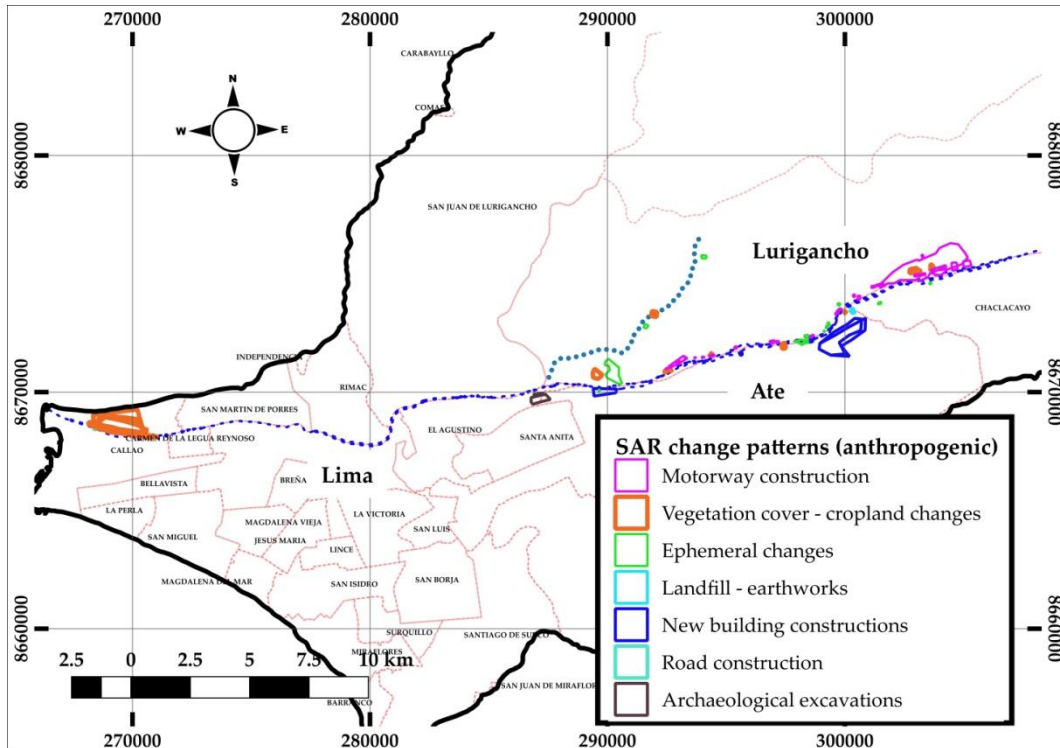
81 The flooded areas concentrate mainly in the district of Lurigancho-Chosica (orange polygons in
 82 Figure 2). This is mainly due to the large residential and commercial sectors that were flooded
 83 during the 16/03/2017 flood event. In particular, in the quarter in Carapongo lying on the right bank
 84 of the Rímac River, east of Av. Las Torres, the Sentinel-1 ratio map shows an increase of radar
 85 backscatter. This outcome can be explained accounting that floodwater was not clear water, but
 86 rather contained solid material transported by the strength of the water flow. Field photographs
 87 published in the media show that, alongside wide flooded areas, there were several areas with
 88 debris accumulation, rubble, uprooted trees, damaged cars and heavy vehicles. This has also likely
 89 contributed to increase both the surface roughness and the soil moisture locally and, therefore,
 90 increase the radar backscatter.

91 Among the radar backscatter change patterns associated to riverbed flooded by increased water
 92 flow, it is worth mentioning those mapped in the downstream sections of the Rímac River. There,
 93 the observed decrease in the radar signal is due to the increase in the water flow and rise in the water
 94 level within the river and typically occurs in correspondence with the transition from the dry to the
 95 rainy season (e.g., between December and March of each year). While these changes have a relative
 96 relevance for the flooding hazard itself (they occur in non-urban areas, with slope $\leq 5^\circ$), and are a
 97 typical consequence of the rainfall events and water excess, they are important to mark the sections
 98 of the river course where waters rise but, depending on the height of the riverbanks, may flow out
 99 and inundate the surrounding land, or not.

100 Figure 3 displays the spatial distribution of the 212 radar backscatter changes (total extent of
 101 26.40 km²) related to the anthropogenic activities that occurred in relation to the periods 1997–1998
 102 and 2017–2018. Of these changes, for the purposes of flooding risk assessment we considered those
 103 whose type and spatial position with respect to the known hazard factors (natural, geological and
 104 anthropogenic) could suggest a potential impact on increasing the risk locally. For example, changes
 105 due to: motorway, new building and road construction.
 106



107
 108 **Figure 2.** Distribution of the areas of the Rímac River basin where change patterns in the radar
 109 backscatter that are likely related with flooding were observed and mapped. Where visible, dashed
 110 lines indicate sections of rivers where no change patterns have been found. Full paper source: [3].



111

112 **Figure 3.** Distribution of changes in the radar backscatter, likely due to human activities
 113 (anthropogenic), observed and mapped within the Rímac River basin. Full paper source: [3].

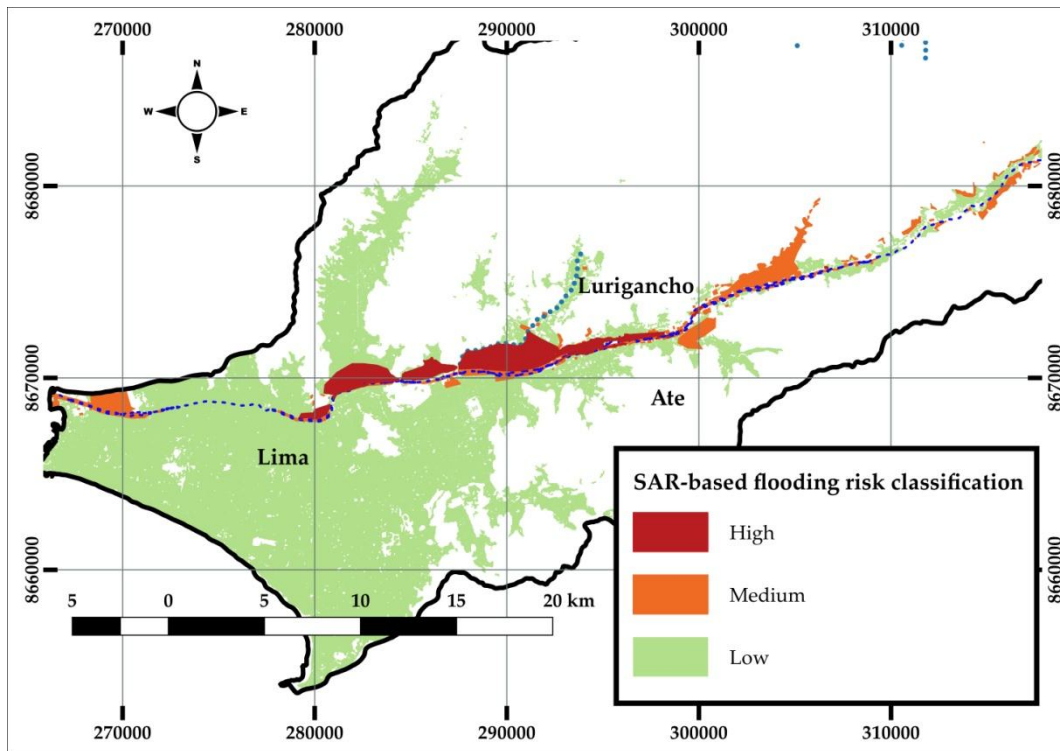
114 **4. Discussion and conclusions**

115 For the generation of the Rímac River basin flood risk map, three risk levels were defined: high,
 116 medium and low risk. The factors determining the level category were, first of all, the terrain slope,
 117 the surface occupied with alluvial deposits, and/or the presence of urban or non-urban area. With
 118 this approach we found that all the radar backscatter changes with a given significance for flooding
 119 risk assessment are located onto alluvial deposits, their most common slope is $\leq 10^\circ$ [3], and they
 120 split among urban and non-urban areas.

121 The areas identified at a high risk of flooding are those that in the years 1997–1998 and
 122 2017–2018 were directly affected by the flooding event, and where satellite data and/or ground
 123 evidence suggest that material loss occurred (e.g., collapse of riverbanks), slope was $\leq 5^\circ$ or falling
 124 between 6° and 10° , and urban fabric is onto alluvial deposits. The medium risk was attributed to
 125 non-urban areas that could be affected by flooding events as a result of the combination between
 126 slope with values $\leq 10^\circ$ and presence of alluvial deposits. In the end, urban areas where neither
 127 previous evidence of flooding nor changes in the satellite data were found, and where it is very
 128 unlikely that they would be inundated due to their slope characteristics (between 15° and 20°)
 129 and/or local geology, were classified at low risk.

130 Figure 4 displays the resulting map of SAR-based flooding risk assessment. Because this map is
 131 the outcome of combining hazard and risk factors, and the changes (both due to flooding or not)
 132 found in the SAR data, it provides the zoning of the areas at risk with respect to flooding events of
 133 equal or greater magnitude than those occurred in 1997–1998 and 2017–2018, if no hazard and risk
 134 mitigation measures are undertaken. By comparison with hazard and susceptibility maps made
 135 solely based on geological factors (e.g. published by Villacorta et al. [6]), the present map has the
 136 advantage to embed flood event-based information as well as knowledge of the impacts of recent
 137 urbanization within the hazard assessment. Therefore, the information mined from SAR time series
 138 contribute to improve hazard mapping products.

139



140

141 **Figure 4.** Map of flooding risk classification at basin scale over Lima, based on the combination of
 142 satellite SAR evidence and natural and anthropogenic factors of flooding hazard, vulnerability and
 143 exposed elements. Full paper source: [3].

144 While the hydraulic risk map presented in this paper was developed *a posteriori* (i.e. after the
 145 flood events happened), the SAR-based methodology behind it is indeed suitable to be iteratively
 146 applied, should newly acquired SAR images be analyzed and/or other events occur. This means that
 147 this approach can be applied in future for regular monitoring of the Rímac River basin, with the aim
 148 of updating the knowledge and understanding of flood risk factors and the consequent
 149 susceptibility. Such regular mapping of changes (either natural or anthropogenic) is a key element in
 150 the framework of disaster risk management, as it contributes to preparedness, resilience building
 151 and reduction of impacts of such natural hazard events on socio-economic levels.

152 **Acknowledgments:** This research was carried out during the internship of N. Alvan Romero at the Italian
 153 Space Agency (ASI) under the supervision of D. Tapete and F. Cigna, in the framework of the II Level Master in
 154 Space Science and Technology at the University of Rome Tor Vergata (Italy). Copernicus Sentinel-1 data were
 155 sourced from the European Space Agency (ESA)'s Copernicus Open Access Hub, while ERS-1/2 data were
 156 accessed through EOLi-SA (project ID 45250). Global Urban Footprint (GUF) product over Lima was provided
 157 by the German Aerospace Center (DLR).

158 **Author Contributions:** Conceptualization, D.T. and F.C.; methodology, N.A.R.; formal analysis, N.A.R.;
 159 resources, D.T. and F.C.; data curation, N.A.R.; writing—original draft preparation, N.A.R.; writing—review
 160 and editing, D.T. and F.C.; supervision, D.T. and F.C. All authors have read and agreed to the published
 161 version of the manuscript.

162 **Conflicts of Interest:** The authors declare no conflict of interest.

163 References

- 164 1. Chávez Cresta, J. L.; Burbano, C.; Villalobos, M. G. *Fortaleciendo la respuesta ante desastres en el Perú: Lecciones*
 165 *Aprendidas del Fenómeno El Niño Costero 2017 en el Perú*; WFP, W. F. P., Children, S. the, USAID, U. S. A. for I.
 166 D., Eds.; INDECI, Instituto Nacional de Defensa Civil; WFP, World Food Programme; Save the Children;
 167 USAID, US Agency for International Development: Breña, Lima-Peru, 2018;

- 168 2. EM-DAT; Guha-Sapir, D. The Emergency Events Database.
169 3. Alvan Romero, N.; Cigna, F.; Tapete, D. ERS-1/2 and Sentinel-1 SAR Data Mining for Flood Hazard and
170 Risk Assessment in Lima, Peru. *Appl. Sci.* **2020**, *10*, 6598, doi:10.3390/app10186598.
171 4. ERS - Earth Online - ESA Available online:
172 <https://earth.esa.int/web/guest/missions/esa-operational-eo-missions/ers> (accessed on Sep 10, 2020).
173 5. ESA Sentinel-1: ESA's Radar Observatory Mission for GMES Operational Services Available online:
174 https://sentinel.esa.int/documents/247904/349449/S1_SP-1322_1.pdf.
175 6. Villacorta Chambi, S. P.; Núñez Juárez, S.; Vásquez Acuña, J.; Pari Pinto, W.; Ochoa Zubiata, M. B.;
176 Benavente Escobar, C. L.; Tatar, L.; Luque Poma, G.; Rosado Seminario, M.; Fídel Smoll, L.; Úbeda
177 Palenque, J. *INGEMMET, Boletín Serie C: Geodinámica e Ingeniería Geológica; Boletín 59: Peligros Geológicos En*
178 *El área De Lima Metropolitana Y La Región Callao*; 2015;



© 2020 by the authors; licensee MDPI, Basel, Switzerland. This article is an open access article distributed under the terms and conditions of the Creative Commons by Attribution (CC-BY) license (<http://creativecommons.org/licenses/by/4.0/>).